Reduction of the Dark-Current in Carbon Nanotube Photo-Detectors

M. Pourfath, H. Kosina, and S. Selberherr
Institute for Microelectronics, TU Wien
Gusshausstrasse 27–29, 1040 Vienna, Austria
Email: {pourfath|kosina|selberherr}@iue.tuwien.ac.at

***Abstract*—Carbon nanotubes have been considered in recent years for future opto-electronic applications because of their direct band-gap and the tunability of the band-gap with the CNT diameter. The performance of infra-red photo-detectors based on carbon nanotube field-effect transistors is analyzed, using the non-equilibrium Green's function formalism. The relatively low ratio of the photo-current to the dark current limits the performance of such devices. We show that by employing a double gate structure this ratio can be significantly increased.**

Carbon nanotubes (CNTs) have been extensively studied in recent years due to their exceptional electronic, opto-electronic, and mechanical properties. CNTs can be considered as a graphene sheet which has been wrapped into a tube. The way the graphene sheet is wrapped is represented by a pair of indices (n, m) called the chiral vector. The integers n and m denote the number of unit vectors along two directions in the honeycomb crystal lattice of graphene. If $m = 0$, the CNT is called *zigzag*. If $n = m$, the CNT is called *armchair*. Otherwise, it is called *chiral*. CNTs with $n-m = 3$ are metals, otherwise they are semiconductors. Semiconducting CNTs can be used as channels for transistors. Depending on the work function difference between the metal contact and the CNT, carriers at the metal-CNT interface encounter different barrier heights. Fabrication of devices with positive [1] and zero [2] barrier heights for holes have been reported. In this work we consider symmetric barrier heights for electrons and holes.

Some of the interesting electronic properties of CNTs are quasi-ballistic carrier transport [2], suppression of short-channel effects due to one-dimensional electron transport [3], and a nearly symmetric structure of the conduction and valence bands, which is advantageous for complementary circuits. Moreover, owing to excellent optical properties of CNTs, an all-CNT electronic and opto-electronic circuit can be envisioned. The direct band-gap and the tunability of the band-gap with the CNT diameter renders them as suitable candidates for opto-electronic devices, especially for infra-red (IR) applications [4, 5] due to the relatively narrow band gap.

IR photo detectors based on carbon nanotube field effect transistors (CNT-FETs) have been reported in [5–7]. To explore the physics of such devices self-consistent quantum mechanical simulations have been performed. The performance of IR photo detectors based on CNT-FETs is analyzed numerically, employing the non-equilibrium Green's function formalism (NEGF). This method has been successfully utilized to investigate the characteristics of CNT-FETs [8–11]. To extend our previous work [12], we employed the NEGF method based on the tight-binding π-bond model to study quantum transport in IR photo detectors based on CNT-FETs and investigate methods to improve the performance of such devices.

The outline of the paper is as follows. In Section I, the NEGF formalism is briefly described. The implementation of this method for CNT-FETs is presented in Section II. In Section III single-gate and double-gate device responses are studied. Finally, conclusions are drawn in Section IV.

I. Non-equilibrium Green's Function Formalism

The NEGF formalism initiated by Schwinger, Kadanoff, and Baym allows to study the time evolution of a many-particle quantum system. Knowing the single-particle Green's functions of a given system, one may evaluate single-particle quantities such as carrier density and current. The many-particle information about the system is cast into self-energies, which are part of the equations of motion for the Green's functions. A perturbation expansion of the Green's functions is the key to approximate the self-energies. Green's functions enable a powerful technique to evaluate the properties of a many-body system both in thermodynamic equilibrium and non-equilibrium situations.

Four types of Green's functions are defined as the non-equilibrium statistical ensemble averages of the single particle correlation operator. The greater Green's function $G^{>}$ and the lesser Green's function $G^{<}$ deal with the statistics of carriers. The retarded Green's function G^{R} and the advanced Green's function G^{A} describe the dynamics of carriers.

Under steady-state condition the equation of motion for the Green's functions can be written as:

$$[E - H]\, G^{\mathrm{R,A}}(1,2) - \int d3\ \Sigma^{\mathrm{R,A}}(1,3) G^{\mathrm{r,a}}(3,2) = \delta_{1,2} \tag{1}$$

$$G^{\lessgtr}(1,2) = \int d3 \int d4\ G^{\mathrm{R}}(1,3) \Sigma^{\lessgtr}(3,4) G^{\mathrm{A}}(4,2) \tag{2}$$

The abbreviation $1 \equiv (\mathbf{r_1}, t_1)$ is used. H is the single-particle Hamiltonian operator, and Σ^{R}, $\Sigma^{<}$, and $\Sigma^{>}$ are the retarded, lesser, and greater self-energies, respectively.

978-1-4244-2363-7/08/$25.00 ©2008 IEEE.

II. Implementation

This section describes the implementation of the outlined NEGF formalism for the numerical analysis of CNT-FETs. A tight-binding Hamiltonian is used to describe transport phenomena in CNT-FETs. The self-energy due to electron-photon interactions are studied next.

A. Tight-Binding Hamiltonian

In graphene three σ bonds hybridize in an sp^2 configuration, whereas the other $2p_z$ orbital which is perpendicular to the graphene layer, forms π covalent bonds. The π energy bands are predominantly determining the solid state properties of graphene. Similar considerations hold for CNTs. We use a nearest-neighbor tight-binding π-bond model [8]. Each atom in an sp^2-coordinated CNT has three nearest neighbors, located $a_{\rm cc} = 1.42$ Å away. The band-structure consists of π-orbitals only, with the hopping parameter $t = V_{pp\pi} \approx -2.7$ eV and zero on-site potential.

The tight-binding Hamiltonian matrix for a $(n, 0)$ zigzag CNT, shown in Fig. 1-a, can be written as [8]

$$\underline{H} = \begin{pmatrix} \underline{U_1} & \underline{t_1} & & & \\ \underline{t_1} & \underline{U_2} & \underline{t_2} & & \\ & \underline{t_2}^\dagger & \underline{U_3} & \underline{t_1} & \\ & & \underline{t_1} & \underline{U_4} & . \\ & & & . & . \end{pmatrix} \tag{3}$$

where the underlined quantities denote matrices. We assume that the electrostatic potential shifts the on-site potential. Therefore, $\underline{U_i}$ is a diagonal matrix which represents the electrostatic potential energy in the ith circumferential ring of carbon atoms. Equal electrostatic potential for all carbon atoms within a ring is assumed, therefore $\underline{U_i} = U_i \underline{I}$. The first and second kind of interaction matrix between the neighboring rings are denoted by $\underline{t_1}$ and $\underline{t_2}$. Only the nearest neighbor interaction between carbon atoms is considered. The coupling matrix between layer 2 and layer 3 is diagonal, $\underline{t_1} = t\,\underline{I}$, where t is the hopping parameter. However, the coupling matrix between layer 1 and layer 2 is given by

$$\underline{t_2} = \begin{pmatrix} t & & & t \\ t & t & & \\ & t & t & \\ & & . & . \end{pmatrix} \tag{4}$$

The eigen vectors of the matrix $\underline{t_2}$ represent plane waves around the circumference of the CNT with the quantized wave-vectors $k_\nu = 2\pi\nu/\sqrt{3}a_{\rm cc}n$, where $\nu = 1, 2, \ldots n$ [8], and the eigen values $2t\cos(\pi\nu/n)$. By transforming from real space into eigen mode space [13], the subbands become decoupled and the Hamiltonian can be written as $\underline{H} = \sum_\nu \underline{H}^\nu$, where $\underline{H}^\nu$, the Hamiltonian of the subband ν is non-diagonal, given by

$$\mathbf{H}^\nu = \begin{pmatrix} U_1^\nu & t_1^\nu & & & \\ t_1^\nu & U_2^\nu & t_2^\nu & & \\ & t_2^\nu & U_3^\nu & t_1^\nu & \\ & & t_1^\nu & U_4^\nu & . \\ & & & . & . \end{pmatrix} \tag{5}$$

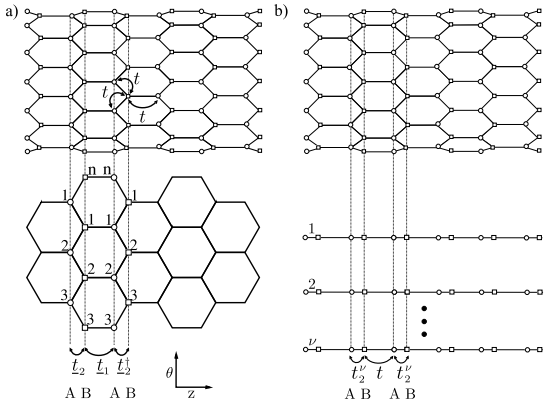

Fig. 1: Layer layout of a $(n, 0)$ zigzag CNT. a) The coupling matrices between layers are denoted by $\underline{t_1}$ and $\underline{t_2}$, where $\underline{t_1}$ is a diagonal matrix and $\underline{t_2}$ includes off-diagonal elements. b) The corresponding one-dimensional chain, in mode space, with two sites per unit cell with hopping parameters t and $t_2^\nu = 2t\cos(\pi\nu/n)$.

Here $U_i^\nu = U_i$, $t_1^\nu = t$, and $t_2^\nu = 2t\cos(\pi\nu/n)$ [8, 9]. The one-dimensional tight-binding Hamiltonian $\underline{H}^\nu$ describes a chain with two sites per unit cell with on-site potential U_i^ν and hopping parameters t and t_2^ν, see Fig. 1-b.

B. Electron-Photon Self-Energies

The Hamiltonian of the electron-photon interaction can be written as [14, 15]:

$$\hat{H}_{e-ph} = \sum_{l,m} M_{l,m} \left(\hat{b} e^{-i\omega t} + \hat{b}^\dagger e^{+i\omega t} \right) \hat{a}_l^\dagger \hat{a}_m \tag{6}$$

$$M_{l,m} = (z_m - z_l)\,\frac{i\mathrm{e}}{\hbar}\,\sqrt{\frac{\hbar I_\omega}{2N\omega\epsilon c}}\langle l|\hat{H}_0|m\rangle \tag{7}$$

where z_m denotes the position of the carbon atom at site m (Fig. 1-a), I_ω is the flux of photons with the frequency ω, and N is the photon population number. The incident light is assumed to be monochromatic, with polarization along the CNT axis, see Fig. 2-a.

We employed the lowest order self-energy of the electron-photon interaction based on the self-consistent Born approximation [16]:

$$\begin{aligned} \Sigma_{l,m}^{<,\nu}(E) &= \textstyle\sum_{p,q} M_{l,p} M_{q,m} \\ &\times \left[N G_{p,q}^{<,\nu}(E - \hbar\omega) + (N+1) G_{p,q}^{<,\nu}(E + \hbar\omega) \right] \end{aligned} \tag{8}$$

where the first term corresponds to the excitation of an electron by the absorption of a photon and the second term corresponds to the emission of a photon by de-excitation of an electron. The transport equations must be iterated to achieve convergence of the electron-phonon self-energies, resulting in a self-consistent Born approximation.

C. Current

The current density at the edge between the nodes l and $l+1$ is given by

$$j_{l,l+1} = \frac{4\mathrm{q}}{\hbar} \sum_\nu \int \frac{dE}{2\pi} 2\Re\mathrm{e}\{G_{l,l+1}^{<,\nu}(E) t_{l+1,l}^\nu\} \tag{9}$$

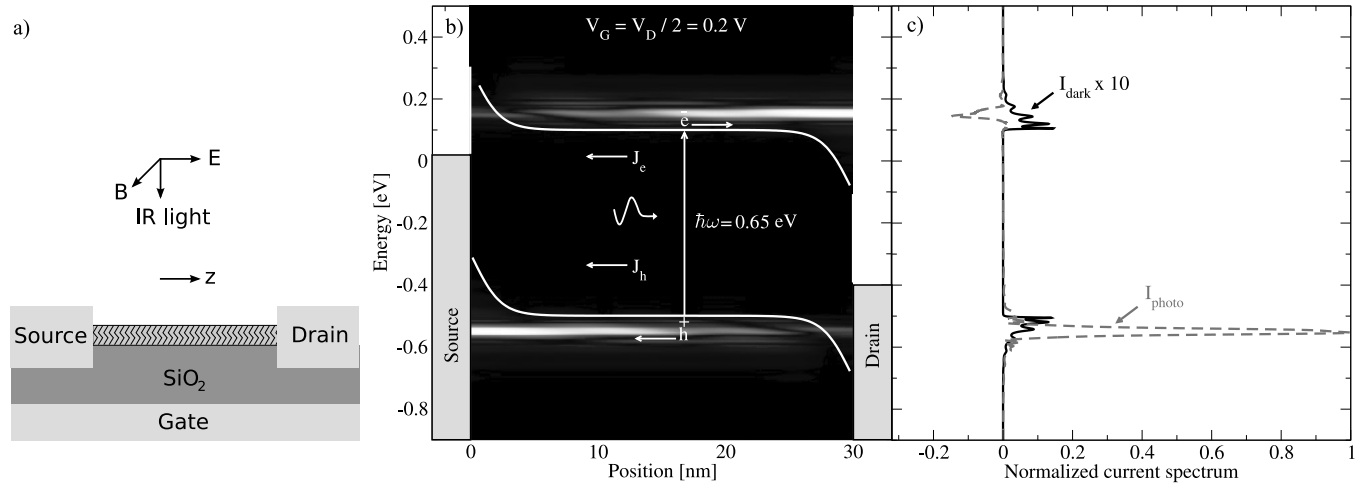

Fig. 2: a) The sketch of a single gate (SG) CNT-FET. Parameters are $t_{\rm oxide} = 2$ nm and $L_{\rm CNT} = 30$ nm. A bottom gate geometry is assumed. b) The spectrum of the current in the channel of a SG CNT-FET. Incident photons generate electron-hole pairs and the electric field drives electrons and holes towards the drain and source contacts, respectively. $E_{\rm G} = 0.6$ eV, $\hbar\omega = 0.65$ eV, and $V_{\rm G} = V_{\rm D}/2 = 0.2$ V. c) The spectrum of the current at the source contact. The red-solid line shows the photo-current spectrum and the black-dashed line the dark-current spectrum which is scaled by a factor of 10.

where the factor 4 is due to the spin and band degeneracy. An adaptive method for selecting the energy grid has to be used to accurately resolve fine resonances at some energies in (9) [17].

III. Simulation Results

First we consider a single gate (SG) CNT-FET IR photo-detector (Fig. 2-a). The spectrum of the current is shown in Fig. 2-b. Incident photons generate electron-hole pairs and the electric field drives electrons and holes to the drain and source contacts, respectively. The photo-current at the source contact is mostly due to the drift of the photo-generated holes towards the source contact. However, there is a small reverse electron current due to tunneling of photo-generated electrons back to the source contact, see Fig. 2-c.

Apart from the photo-current there is a non-wanted dark current due to thermionic emission and tunneling of carriers from the contacts to the channel. For a SG device the maximum ratio of the photo-current to the dark-current can reach $I_{\rm photo}/I_{\rm dark} \approx 20$, which may not be sufficient for many applications. To reduce the dark-current we suggest a double gate (DG) structure (Fig. 3-a). We have previously shown that by employing a DG design, carrier injection at the source and drain contacts of an CNT-FET can be separately controlled [12]. Here, we extend our previous work and study a DG device for the detection of IR photons.

In a DG CNT-FET the band-edge profile near the contacts can be controlled by the gate voltages [12]. We consider the bias condition $V_{\rm G1} = V_{\rm S} - \Delta V$ and $V_{\rm G2} = V_{\rm D} + \Delta V$, where ΔV is some offset voltage. In a DG device, similar to a SG one, the electric field along the channel drives electrons towards the drain and holes towards the source contact. However, if $\Delta V > 0$ the local electric field close to the contacts reverses the sign, see Fig. 3-b. Under this condition the parasitic thermionic emission and tunneling of carriers from the contacts to the channel is strongly suppressed. As shown in Fig. 4, the parasitic dark-current decreases as ΔV increases. However, the dark-current increases again for $\Delta V > 0.1$ V because of the increase of the band to band tunneling current due to the increase of the electric field.

If $\Delta V > 0$ the local electric field drives photo-generated electrons and holes towards the source and drain contacts, respectively, which increases the reverse photo-current. As a result, as shown in Fig. 4, by increasing ΔV the total photo-current is slightly reduced, whereas the dark current is strongly reduced. Our results indicate that for the given structure and drain voltage at $\Delta V \approx 0.07$ V the ratio of the photo-current to the dark-current can reach a maximum value of $I_{\rm photo}/I_{\rm dark} \approx 2 \times 10^5$, which implies a considerable improvement of the device characteristics.

IV. Conclusions

The performance of IR photo detectors based on CNT-FETs was investigated. The coupled system of transport and Poisson equations was solved self-consistently. A tight-binding Hamiltonian is used to describe transport phenomena in CNT-FETs. In agreement with experimental data, our results indicate that the ratio of the photo-current to the dark-current is relatively low. However, we suggest that by employing a DG structure the dark-current can be significantly decreased, whereas the photo-current remains nearly unchanged. Our results show that by appropriate selection of the two gate voltages the ratio of the photo-current to the dark-current can be maximized.

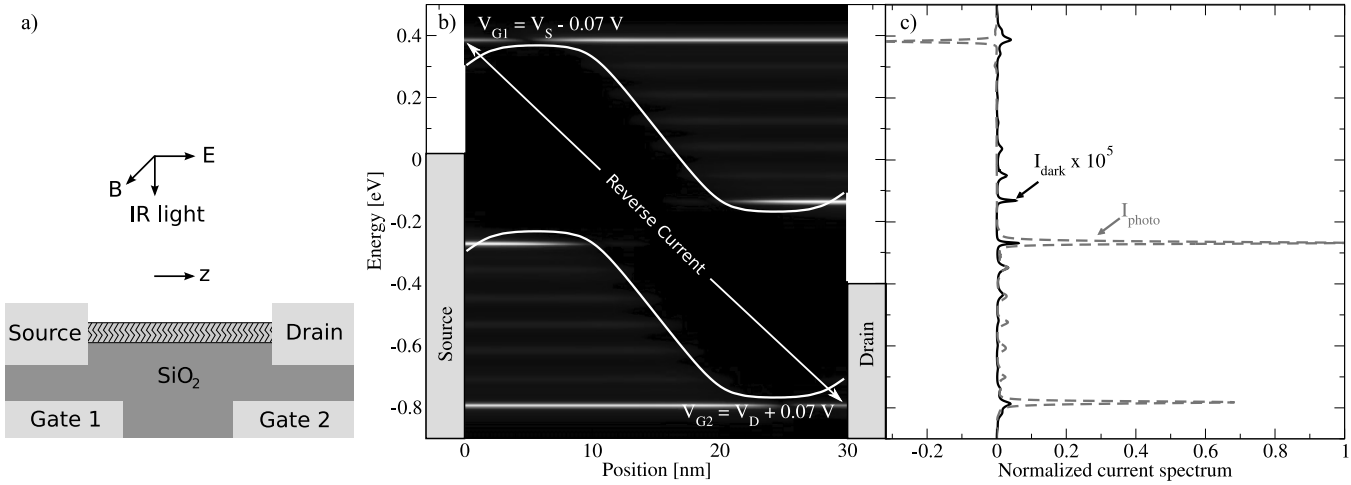

Fig. 3: a) The sketch of a double gate (DG) CNT-FET. $L_{\rm G1} = L_{\rm G2} = 10$ nm. b) The spectrum of the current along the channel of a DG CNT-FET. $\Delta V = 0.07$ V and $V_{\rm D} = 0.4$ V. c) The spectrum of the current at the source contact. The solid line shows the photo-current spectrum and the dashed line the dark-current spectrum which is scaled by a factor of 10^5.

ACKNOWLEDGMENT

This work, as part of the European Science Foundation EUROCORES Programme FoNE, was supported by funds from FWF (Contract I79-N16), CNR, EPSRC and the EC Sixth Framework Programme, under Contract No. ERAS-CT-2003-980409.

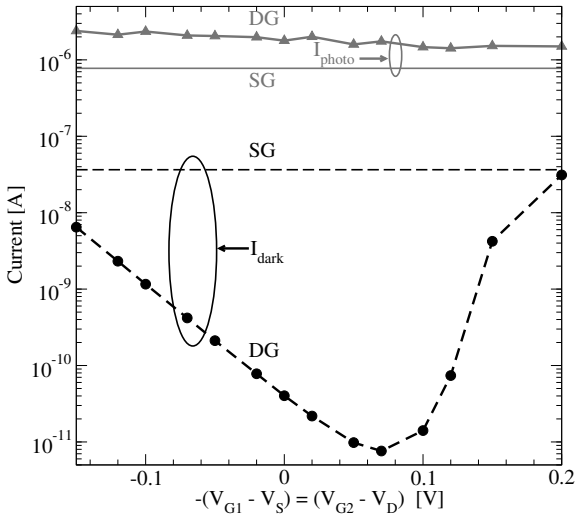

Fig. 4: The effect of the gate voltage offset ΔV on the photo-current and dark-current of a DG CNT-FET IR detector. Both the photo-current and the dark-current of a SG devices is shown for comparison.

REFERENCES

[1] J. Appenzeller, M. Radosavljevic, J. Knoch, and P. Avouris, "Tunneling Versus Thermionic Emission in One-Dimensional Semiconductors," *Phys. Rev. Lett.*, vol. 92, p. 048301, 2004.

[2] A. Javey, J. Guo, Q. Wang, M. Lundstrom, and H. Dai, "Ballistic Carbon Nanotube Field-Effect Transistors," *Nature (London)*, vol. 424, no. 6949, pp. 654–657, 2003.

[3] J.-Y. Park, "Carbon Nanotube Field-Effect Transistor with a Carbon Nanotube Gate Electrode," *Nanotechnology*, vol. 18, no. 9, p. 095202, 2007.

[4] M. Freitag, J. Chen, J. Tersoff, J. Tsang, Q. Fu, J. Liu, and P. Avouris, "Mobile Ambipolar Domain in Carbon-Nanotube Infrared Emitters," *Phys. Rev. Lett.*, vol. 93, p. 076803, 2004.

[5] M. Freitag, Y. Martin, J. Misewich, R. Martel, and P. Avouris, "Photoconductivity of Single Carbon Nanotubes," *Nano Lett.*, vol. 3, no. 8, pp. 1067–1071, 2003.

[6] S. Lu and B. Panchapakesan, "Photoconductivity in Single Wall Carbon Nanotube Sheets," *Nanotechnology*, vol. 17, no. 8, pp. 1843–1850, 2006.

[7] J. Zhang, N. Xi, H. Chan, and G. Li, "Single Carbon Nanotube Based Infrared Sensor," *Proc. SPIE*, vol. 6395, p. 63950A, 2006.

[8] J. Guo, S. Datta, M. Lundstrom, and M. Anantram, "Multi-Scale Modeling of Carbon Nanotube Transistors," *Intl. J. Multiscale Comput. Eng.*, vol. 2, no. 2, pp. 257–278, 2004.

[9] A. Svizhenko and M. Anantram, "Effect of Scattering and Contacts on Current and Electrostatics in Carbon Nanotubes," *Phys. Rev. B*, vol. 72, p. 085430, 2005.

[10] M. Pourfath, H. Kosina, and S. Selberherr, "Rigorous Modeling of Carbon Nanotube Transistors," *IOP J. Phys.: Conf. Ser.*, vol. 38, pp. 29–32, 2006.

[11] M. Pourfath and H. Kosina, "The Effect of Phonon Scattering on the Switching Response of Carbon Nanotube FETs," *Nanotechnology*, vol. 18, pp. 424 036–6, 2007.

[12] M. Pourfath, A. Gehring, E. Ungersboeck, H. Kosina, S. Selberherr, B.-H. Cheong, and W. Park, "Separated Carrier Injection Control in Carbon Nanotube Field-Effect Transistors," *J. Appl. Phys.*, vol. 97, no. 10, pp. 106 103–3, 2005.

[13] R. Venugopal, Z. Ren, S. Datta, M. Lundstrom, and D. Jovanovic, "Simulating Quantum Transport in Nanoscale Transistors: Real Versus Mode-Space Approaches," *J. Appl. Phys.*, vol. 92, no. 7, pp. 3730–3739, 2002.

[14] E. Lindor and E. Henrickson, "Nonequilibrium Photocurrent Modeling in Resonant Tunneling Photodetectors," *J. Appl. Phys.*, vol. 91, no. 10, pp. 6273–6281, 2002.

[15] D. A. Stewart and F. Leonard, "Photocurrents in Nanotube Junctions," *Phys. Rev. Lett.*, vol. 93, no. 10, p. 107401, 2004.

[16] R. Lake, G. Klimeck, R. C. Bowen, and D. Jovanovic, "Single and Multiband Modeling of Quantum Electron Transport Through Layered Semiconductor Devices," *J. Appl. Phys.*, vol. 81, no. 12, pp. 7845–7869, 1997.

[17] M. Pourfath and H. Kosina, "A Fast and Stable Poisson-Schrödinger Solver for the Analysis of Carbon Nanotube Transistors," *J. Comp. Electronics*, vol. 5, no. 2-3, pp. 155–159, 2006.